

Multi-shot NAS for Discovering Adversarially Robust Convolutional Neural Architectures at Targeted Capacities

Xuefei Ning* Junbo Zhao* Wenshuo Li Tianchen Zhao Huazhong Yang
Yu Wang

Department of Electronic Engineering, Tsinghua University
foxdoraame@gmail.com, zhaojunbo2012@sina.cn, yu-wang@tsinghua.edu.cn

Abstract

Convolutional neural networks (CNNs) are vulnerable to adversarial examples, and studies show that increasing the model capacity of an architecture topology (e.g., width expansion) can bring consistent robustness improvements. This reveals a clear robustness-efficiency trade-off that should be considered in architecture design. Recent studies have employed one-shot neural architecture search (NAS) to discover adversarially robust architectures. However, since the capacities of different topologies cannot be easily aligned during the search process, current one-shot NAS methods might favor topologies with larger capacity in the supernet. And the discovered topology might be sub-optimal when aligned to the targeted capacity. This paper proposes a novel multi-shot NAS method to explicitly search for adversarially robust architectures at a certain targeted capacity. Specifically, we estimate the reward at the targeted capacity using inter- or extra-polation of the rewards from multiple supernets. Experimental results demonstrate the effectiveness of the proposed method. For instance, at the targeted FLOPs of 1560M, the discovered MSRobNet-1560 (clean 84.8%, PGD¹⁰⁰ 52.9%) outperforms the recent NAS-discovered architecture RobNet-free (clean 82.8%, PGD¹⁰⁰ 52.6%) with similar FLOPs.

1. Introduction

Convolutional neural networks (CNNs) are known to be vulnerable to adversarial examples (a.k.a., adversarially crafted imperceptible perturbations) [30]. For defending against adversarial examples, extensive efforts are devoted to designing training or regularization techniques [6, 16, 31] and introducing special modules (e.g., randomness injection [8], generative model [27, 28]). On the other hand, only a few studies explored the robustness characteristics from the architectural aspect.

As been reported by previous studies [16], increasing the capacity of a topology (e.g., width expansion) brings consistent robustness improvements. According to the observation, one can simply enlarge the architecture’s width to achieve higher robustness at the cost of increasing model capacity. Nevertheless, in actual deployment, a capacity budget requirement on the architecture can exist, and we propose a novel multi-shot neural architecture search (NAS) method to explicitly **search for adversarially-robust architectures at the targeted capacities**.

Currently, parameter-sharing techniques are widely used in NAS methods to boost search efficiency [24, 14]. In parameter-sharing NAS, a supernet is constructed such that all architectures in the search space are sub-architectures of this supernet. Then, during the search process, each candidate architecture can be evaluated using the weights in the supernet without a separate training phase. After the search, a topology is derived, and model augmentation along the width or depth dimension is usually applied to construct a larger final architecture. One-shot NAS is a specific type of parameter-sharing NAS methods, in which the supernet training phase and search phase are decoupled.

The challenge of applying one-shot NAS to discover the superior topologies at certain targeted capacities lies in that the model capacity of different topologies cannot be aligned in the supernet. As illustrated in Fig. 1, a topology (Topology 2) is discovered by one-shot NAS since it has a high one-shot reward. However, another topology (Topology 1) with a lower one-shot reward and lower one-shot capacity (reward/capacity in the supernet) might be better when these topologies are aligned to the same capacity.

In this paper, we address the evaluation gap introduced by the capacity dis-alignment issue. Specifically, we inter- or extra-polating the performances evaluated by multiple supernets of different sizes (a.k.a., multi-shot NAS) to estimate the reward at the targeted capacity. Experimental results on CIFAR-10 show that at the targeted capacities, the discovered MSRobNet architectures outperform manually-designed ones and those discovered by vanilla one-shot

*Equal contribution.

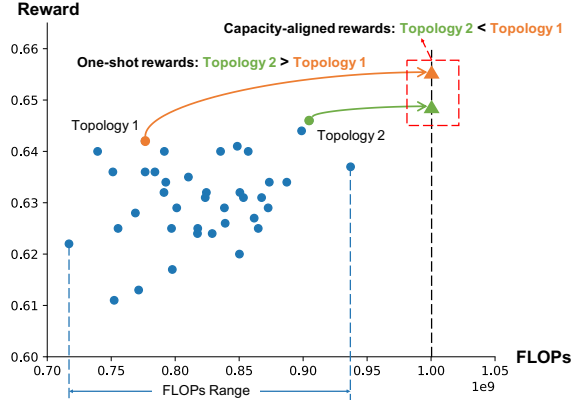


Figure 1. A motivating illustration. The FLOPs range of different topologies in supernet can be large. When evaluated in the supernet, topology 2 (green) is better than topology 1 (orange). However, when aligned to the same capacity, topology 1 (orange) is better than topology 2 (green).

NAS workflow. The transferability of the architectures to CIFAR-100, SVHN, and Tiny-ImageNet is also verified.

The paper is organized as follows. Sec. 2 summarizes the related studies on adversarial robustness and neural architecture search. Then, we describe the one-shot NAS workflow and its capacity misalignment issue in Sec. 3. And then, we give out the problem definition of NAS for adversarial robustness at targeted capacity in Sec. 4, and our multi-shot architecture search method in Sec. 5. Finally, we show the experimental results and conclude our method in Sec. 6 and Sec. 7.

2. Related Work

2.1. Adversarial Attacks and Defenses

Adversarial Attacks Current studies usually run adversarial attacks to evaluate the robustness of models. Commonly used white-box attacking methods can be classified into local approximation based ones and optimization based ones. Local approximation based methods craft adversarial inputs by following update rules derived with certain local approximations, including the fast gradient sign method (FGSM) and its variants [7, 12], saliency-based [22] methods, local decision boundary method [18]. On the other hand, optimization-based attacking methods formulate the attack as one or multiple optimization problems and solve the optimization problems approximately, of which the most popular ones are the C&W attack and its variants [4, 3].

Adversarial Defenses Existing adversarial defenses can be classified into several categories: 1) adversarial example detection [17, 3]; 2) input mapping or processing [28, 8]; 3) regularization techniques [23, 6]; 4) adversarial training [16, 31]. Among the extensive literature, many defenses

are proved to be not useful to stronger attacks [3, 1], and adversarial training is acknowledged as the most effective defense technique.

Robust CNN Architecture Design In contrast to the aforementioned defenses, we aim to improve the adversarial robustness of CNNs from the architectural aspect by designing more robust neural architectures. The two most related studies to our work are 1) Guo et al. [9] employed one-shot NAS to investigate the architecture patterns that are beneficial to adversarial robustness, and find that densely connected pattern is beneficial. They analyzed architectures in three coarsely-partitioned capacity range (i.e., small, medium, large), by randomly sampling 100 architecture for each range. In contrast, we develop the multi-shot evaluation strategy to estimate the reward **at a certain capacity**, and conduct guided search using the estimated reward. 2) Chen et al. [5] employed an anti-bandit algorithm to improve the search efficiency. To accelerate the search process, they employed FGSM adversarial training in the search process, while the final model robustness is evaluated with PGD attacks. In our experiment, we found that using FGSM adversarial training during the search process will result in uncorrelated evaluation (See Fig. 4 and Sec. 5.3).

2.2. Neural Architecture Search

Problem Definition Neural architecture search has been recently employed to automatically discover neural architectures for various tasks [32, 24, 14, 26]. The basic formalization of the NAS problem is in Eq. 1, and many studies focus on approximately solving this problem efficiently.

$$\begin{aligned} \max_{\alpha \in \mathcal{A}} \quad & E_{x_v \sim D_v} [R(x_v, \text{Net}(\alpha, w^*(\alpha)))] \\ \text{s.t.} \quad & w^*(\alpha) = \arg\min_w E_{x_t \sim D_t} [L(x_t, \text{Net}(\alpha, w))], \end{aligned} \quad (1)$$

where \mathcal{A} denotes the architecture search space; D_t, D_v denotes the training and validation dataset, respectively; R denotes the evaluated reward used to instruct the search process, and L denotes the loss function for backpropagation during the training of the weights w .

The vanilla NAS algorithm [32] is extremely slow, since thousands of architectures need to be evaluated, and the evaluation of each architecture involves a separate training process to get $w^*(\alpha)$.

Parameter-sharing Techniques and One-shot NAS A widely-used technique to accelerate the evaluation of each individual architecture is to use parameter-sharing techniques [24, 14]. They construct a super network (a.k.a, supernet) such that all architectures in the search space are sub-architectures of the supernet. Then all architectures can be evaluated using a subset of the weights in the supernet. In this way, the training costs of architectures are amortized to only train an over-parametrized supernet.

One-shot NAS [2] is a specific type of parameter-sharing based NAS method, in which the search process is decoupled into two phases: 1) Train a supernet; 2) Search while using the supernet weights to evaluate candidate architectures without further finetuning.

Predictor-based Controller To reduce the number of architectures needed to be evaluated (a.k.a., improve the sample efficiency of the search process), predictor-based controllers [15, 10, 20] predict the architectures’ performances, and only sample promising architectures. In this way, fewer architectures need to go through the relatively expensive procedure, which includes a separate testing process and sometimes a separate training process.

3. Preliminary: One-shot NAS Workflow

A typical one-shot NAS workflow goes as follows: 1) Train a supernet; 2) Conduct architecture search while using the supernet weights to evaluate candidate architectures. 3) In cell-based search spaces [24, 14], the model augmentation technique (increasing the channel/layer number) is usually applied on the discovered topology to construct a large final architecture. In this paper, we consider the model augmentation in the channel/width dimension. 4) Finally, the augmented architecture is trained on the dataset.

Model capacity has large impacts on the adversarial robustness of a NN model [16, 9]. A natural question is that can we search for superior topology at a certain capacity with one-shot NAS? Unfortunately, since the parameters of different architectures are shared, their capacity cannot be easily aligned. More specifically, the FLOPs of different topologies in supernet can vary in a large range (e.g., for our search space, 304M~1344M in the supernet with 44 init channels), and topologies with larger capacity in the supernet tend to have better one-shot performances. However, these topologies might no longer outperform those with smaller capacity when being augmented to another capacity C_T . A motivating illustration is shown in Fig. 1.

4. Problem Definition

In this paper, we adopt FLOPs (number of floating-point operations) to measure model capacity. Nevertheless, the multi-shot evaluation methodology can be extended to other measures. The problem of searching for an adversarially robust architecture at the targeted capacity C_T can be formalized as in Eq. 2.

$$\begin{aligned}
& \max_{\alpha \in \mathcal{A}} r(\alpha) \\
& \text{s.t. } c(\alpha) = \arg \min_{c \in \mathbb{Z}^+} |C(\text{Aug}(\alpha, c)) - C_T| \\
& w^*(\alpha) = \operatorname{argmin}_w L_t(\alpha, w) \\
& \quad = \operatorname{argmin}_w E_{x_t \sim D_t} [\\
& \quad \max_{x' \in B_p(x_t, \epsilon)} L(x', \text{Net}(\text{Aug}(\alpha, c(\alpha)), w))] \\
& r(\alpha) = E_{x_v \sim D_v} [\min_{x' \in B_p(x_v, \epsilon)} R(x', \text{Net}(\text{Aug}(\alpha, c(\alpha)), w^*(\alpha)))] ,
\end{aligned} \tag{2}$$

where $\text{Aug}(\alpha, c)$ denotes the augmented architecture of topology α with init channel number c ; $C(\text{Aug}(\alpha, c))$ refers to the capacity of the augmented architecture; $c(\alpha)$ is an positive integer found by minimizing the difference of the augmented architecture capacity and the targeted capacity C_T . $B_p(x, \epsilon)$ denotes the ϵ -ball around x under L_p norm, and we can see that both the reward $r(\alpha)$ and the loss $L_t(\alpha, w)$ are calculated in a min-max fashion. Compared with Eq. 1, the reward used for search changes from $E_{x_v \sim D_v} [R(x_v, \text{Net}(\alpha, w^*(\alpha)))]$ to $r(\alpha) = E_{x_v \sim D_v} [\min_{x' \in B_p(x_v, \epsilon)} R(x', \text{Net}(\text{Aug}(\alpha, c(\alpha)), w^*(\alpha)))]$, in which both adversarial robustness and model augmentation are taken in to consideration.

One-shot evaluation is the approximated evaluation strategy for the vanilla NAS problem in Eq. 1: Instead of finding $w^*(\alpha)$ for each topology α , the shared weights in the supernet are used directly to get the approximate one-shot reward. Correspondingly, multi-shot evaluation is the approximated evaluation strategy for the “NAS at targeted capacity” problem in Eq. 2: Instead of actually constructing the augmented network $\text{Net}(\text{Aug}(\alpha, c(\alpha)), \cdot)$ at the targeted capacity C_T and finding its $w^*(\alpha)$, we estimate the targeted reward by inter- or extra-polating multiple one-shot rewards.

5. Multi-shot NAS for Adversarial Robustness

The overall workflow is illustrated in Fig. 2. The multi-shot NAS workflow consist of three steps: 1) Supernet training: Adversarially train K supernet χ_1, \dots, χ_K with init channels c_1^s, \dots, c_K^s , and the corresponding shared weights are w_1, \dots, w_K . A 7-step projected gradient descent attack (PGD⁷) [16] is used for the adversarial training as an approximation of the min-max optimization problem of w_i . 2) Function family selection: Select a extrapolation function family f^* (Sec. 5.2). 3) Architecture search: Explore the search space (Sec. 5.3), and for each candidate topology, the multi-shot evaluation strategy is used to estimate its reward at the targeted capacity C_T (Sec. 5.1).

5.1. Multi-shot Evaluation Strategy

To estimate the reward of a topology α at the targeted capacity C_T , α is firstly evaluated in all K supernet to get

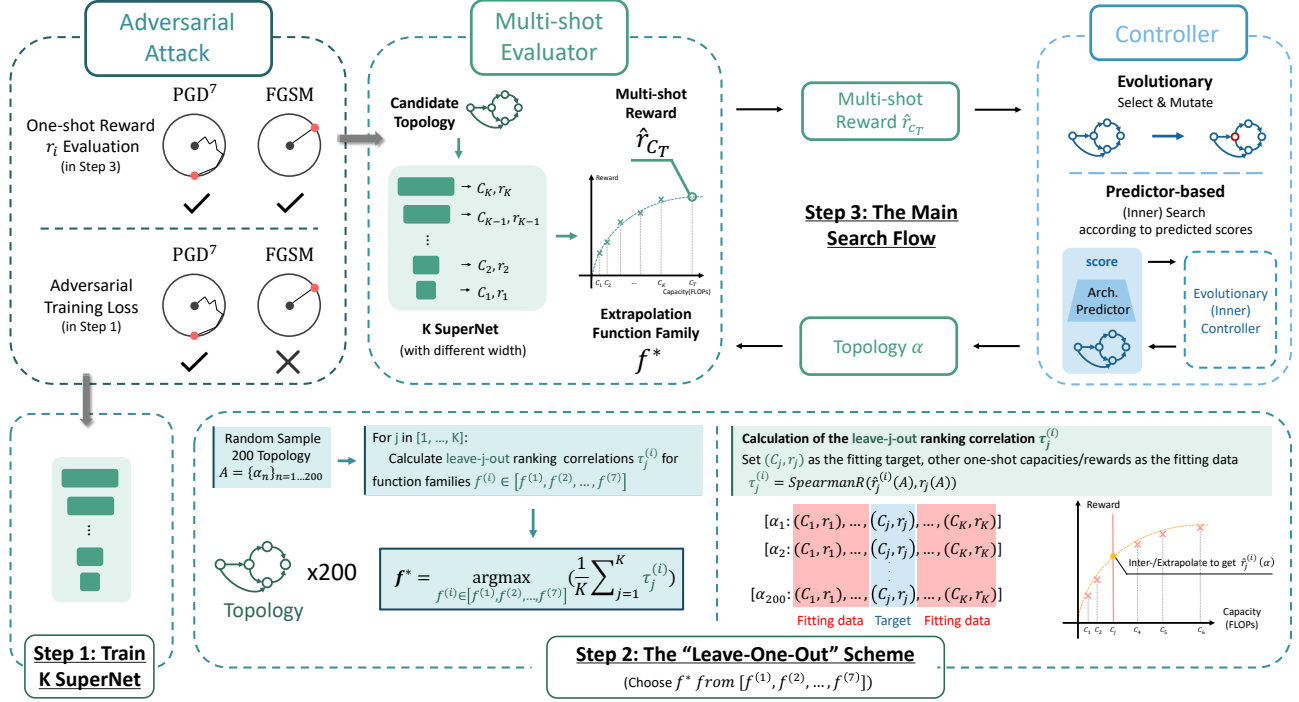


Figure 2. The overall workflow. Step 1: Adversarially train K supernets with PGD⁷ attack. Step 2: Select extrapolation function family f^* based on the average leave-one-out Spearman ranking correlation (Sec. 5.2). Step 3: Conduct architecture search for targeted capacity C_T (Sec. 5.3) using the multi-shot evaluation strategy (Sec. 5.1).

its one-shot rewards $R(\alpha) = \{r_1(\alpha), \dots, r_K(\alpha)\}$. Then, these one-shot rewards together with the corresponding one-shot capacity $C(\alpha) = \{C_1(\alpha), \dots, C_K(\alpha)\}$ are used to fit the extrapolation function family $r = f(C; \beta)$, where β is the parameters. After getting $\hat{\beta} = \text{Fit}(f, R(\alpha), C(\alpha))$ with nonlinear least square fitting, the fitted function is used to estimate the reward \hat{r} at the targeted capacity C_T .

$$\hat{r}_{CT} = f(C_T; \hat{\beta}). \quad (3)$$

One-shot Evaluation and BatchNorm Calibration During each one-shot evaluation, we run PGD⁷ attacks on the validation dataset split and average the clean and adversarial accuracy as the reward $r_i(\alpha)$. Unlike previous studies [9] that train each sub-architecture separately for several epochs, we use the shared weights for sub-architecture evaluation. However, there exist problems with batch normalization (BatchNorm): During the supernet training process, the accumulation of BatchNorm statistics is incorrect for each architecture. Thus, we calibrate BatchNorm statistics using the first 10 batches in the validation split.

5.2. Extrapolation Function Family Selection

Empirical observation [16] shows that as the model capacity gets larger, the increase of the model robustness saturates. Due to this observation, we choose 7 parametric saturating function families and list them in the appendix. After

training K supernets, we select the appropriate extrapolation function family f^* from $F = \{f^{(1)}, \dots, f^{(7)}\}$ by calculating the average leave-one-out ranking correlation, as also illustrated in Fig. 2. More specifically, to assess function family $f^{(i)}(\cdot; \beta)$, for each supernet χ_j , we calculate the leave-j-out ranking correlation $\tau_j^{(i)}$ as follows. For every topology α , we fit the function to get $\beta_j^{(i)}(\alpha)$ while leaving the scores of χ_j out. Then we calculate the Spearman ranking correlation (SpearmanR) between the estimated and actual one-shot rewards of N topologies in χ_j as

$$\begin{aligned} \tau_j^{(i)} &= \text{SpearmanR}(\{\hat{r}_j^{(i)}(\alpha_n)\}_{n=1, \dots, N}, \{r_j(\alpha_n)\}_{n=1, \dots, N}) \\ \text{where } \hat{r}_j^{(i)}(\alpha) &= f_i(\alpha; \beta_j^{(i)}(\alpha)) \\ \beta_j^{(i)}(\alpha) &= \text{Fit}(f^{(i)}, \{r_m(\alpha)\}_{m=1, \dots, K, m \neq j}, \\ &\quad \{C_m(\alpha)\}_{m=1, \dots, K, m \neq j}), \end{aligned} \quad (4)$$

where $N = 200$ random topology samples are used in our experiments. After calculating $\{\tau_j^{(i)}\}_{i=1, \dots, 7, j=1, \dots, K}$, we calculate the average leave-one-out Spearman ranking correlation $\{\bar{\tau}^{(i)}\}_{i=1, \dots, 7}$ for all the candidate function families as in Eq. 5, and choose the function family with the highest $\bar{\tau}^{(i)}$ as the extrapolation family.

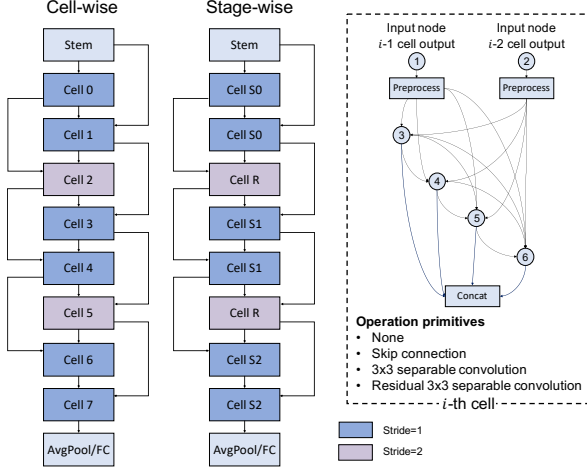


Figure 3. Illustration of the search space. Left: The layout and connection between cells (cell-wise/stage-wise). Right: Densely-connected cell search space. Note that each node can choose arbitrary number of previous nodes in the cell as its inputs, and each cell can have different connections.

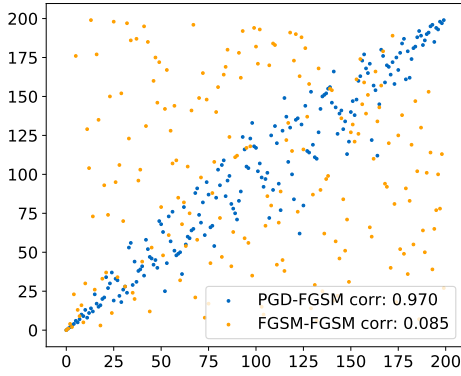


Figure 4. X axis: Indices of architectures sorted according to reward ranking evaluated by PGD⁷-PGD⁷. Y axis: The reward rankings evaluated by PGD⁷-FGSM and FGSM-FGSM. The legends show the Spearman correlation between the rewards and the PGD⁷-PGD⁷ rewards. The supernet’s init channel number is 24.

$$f^* = \arg \max_{f^{(i)} \in F} \bar{\tau}^{(i)} = \arg \max_{f^{(i)} \in F} \sum_{j=1}^K \tau_j^{(i)}. \quad (5)$$

5.3. Search with Multi-shot Evaluation Strategy

After supernet training and function family selection, we explore the search space using the rewards evaluated by the multi-shot evaluation strategy (Sec. 5.1). We conduct multi-shot NAS with two different search strategies (controllers): 1) Evolutionary controller; 2) Predictor-based controller.

5.3.1 Search Space

Fig. 3 summarizes the cell-level search space design and the cell layout. There are four internal nodes in the cell-level search space, and each internal node can choose an arbitrary number of previous nodes as its inputs to enable discovering densely connected patterns [9]. Four primitives are included: none, skip connection, 3x3 separable convolution, residual 3x3 separable convolution. The residual 3x3 separable convolution is a combination of a skip connection and a 3x3 separable convolution.

We experiment with two types of cell layout: cell-wise and stage-wise. In the cell-wise layout, each of the eight cells has a distinct topology, and there are roughly 2.7×10^{67} architectures in the search space. In the stage-wise layout, the cells in each stage share the same topology, and the search space size is enormously reduced to 5.2×10^{33} since only four cell topologies need to be searched.

5.3.2 Evolutionary Search

We use the tournament-based evolutionary search strategy [26] (population size 100, tournament size 10) to explore the cell-wise search space.

5.3.3 Predictor-based Search with Efficient Proxies

To improve the exploration and the efficiency of the search process, we construct a more efficient flow using the following proxies and techniques:

Stage-wise search space: We run the search on the much smaller stage-wise search space, to alleviate poor exploration in the limited search budget. Note that the stage-wise search space is a sub-search-space of the cell-wise one, and no retraining of supernet is needed.

Predictor-based search strategy (controller): We use a predictor-based controller to improve the exploration. Specifically, we use a graph-based encoder [20] to encode the topology of each cell into a continuous embedding, and then concatenate the embeddings of four cell topologies (S0, S1, S2, R) as the architecture embedding. Then the architecture embedding is fed into an MLP to get a predicted score. Based on the predicted scores, promising architectures are selected for the actual multi-shot evaluation. The detailed settings of predictor training and inner search are described in the appendix.

FGSM reward: We use the FGSM attack instead of the PGD⁷ attack to measure the adversarial accuracy. Fig. 4 illustrates the rationality of using FGSM as the proxy reward. The notation “ATTACK1-ATTACK2” means that “ATTACK1” is used in supernet adversarial training, and “ATTACK2” is used in the parameter-sharing evaluation. We can see that as long as a stronger attack (PGD⁷) is

used in adversarial training to avoid gradient masking, the FGSM rewards are highly correlated with the PGD rewards on 200 randomly sampled topologies (SpearmanR=0.97).

Moreover, we only calculate the reward on the first half of the validation split. The FGSM proxy reward and fewer validation images accelerate the evaluation process by roughly $8\times$. And the predictor-based controller enables a better exploration of the reduced stage-wise search space.

6. Experiments

We conduct multi-shot NAS on CIFAR-10, and evaluate the discovered architectures on the CIFAR-10, CIFAR-100, SVHN and Tiny-ImageNet [11, 19] datasets.

6.1. Experimental Setup

6.1.1 Search Settings

During the search process, the original training dataset of CIFAR-10 is divided into two parts: training split (40000 images) and validation split (10000 images). The supernet are trained on the training split, and architecture rewards are evaluated on the validation split.

PGD⁷ with $\epsilon = 0.031(8/255)$ and step size $\eta = 0.0078(2/255)$ is used to approximate the min-max loss in Eq. 2. We train $K = 8$ supernet with init channel number $\{12, 24, 30, 36, 40, 44, 54, 64\}$ for 400 epochs. To train the supernet, we use a batch size of 64, a weight decay of $1e-4$, and an SGD optimizer with momentum 0.9. And the learning rate is set to 0.05 initially and decayed down to 0 following a cosine schedule.

After training K supernet, we select the extrapolation function family with the described method. Then, we use this function family in the search for robust architectures at various targeted FLOPs: 1000M, 1560M, 2000M.

To demonstrate the effectiveness of *multi-shot* NAS in a more controlled setting, we also run several baseline *one-shot* search methods on the cell-wise search space. Denoting $r^{(A)}(\alpha) = \frac{1}{2}(\text{acc}_{\text{adv}} + \text{acc}_{\text{clean}})$, $r^{(B)} = \text{FLOPs}(\alpha)$, the three baseline one-shot search methods are: 1) One-shot-rA: Evolutionary search with reward $r^{(A)}(\alpha)$; 2) One-shot-div: Evolutionary search with a simple scalarized reward $r(\alpha) = r^{(A)}(\alpha)/r^{(B)}(\alpha)$. 3) One-shot-pareto: Considering FLOPs as an objective, run pareto-front-based evolutionary search with the three objectives $\text{acc}_{\text{adv}}, \text{acc}_{\text{clean}}, r^{(B)}$. Compared with one-shot-rA, the latter two search methods prefer architectures with smaller one-shot capacity (FLOPs), which might be beneficial for the architecture performance at certain targeted capacity.

All the one-shot searches are conducted on the supernet with init channel number 44. After the search, the discovered topology is augmented to the targeted capacity C_T .

6.1.2 Adversarial Training and Testing

For the final comparison of all the architectures on CIFAR-10, CIFAR-100 and SVHN, we adversarially train them for 110 epochs using PGD⁷ attacks with $\epsilon = 0.031(8/255)$ and step size $\eta = 0.0078(2/255)$, and other settings are also kept the same for all architectures. More detailed adversarial training settings on CIFAR-10, CIFAR-100, SVHN, and Tiny-ImageNet are elaborated in the appendix.

To evaluate the adversarial robustness of the trained models, we apply the Fast Gradient Sign Method (FGSM) [7] with $\epsilon = 0.031(8/255)$ (4/255 for Tiny-ImageNet) and PGD [16] with different step numbers. On CIFAR-10, we also apply another two attacks that report the successful attacking L_∞ distances using the Foolbox toolbox V2.4.0 [25] and its default settings, and report the median attacking distance on the test dataset: 1) Deep-Fool [18] with at most 100 steps; 2) Basic Iterative Method (BIM) [13] with 20 binary search steps.

6.2. Function Family Selection

The leave-one-out ranking correlations of different candidate function families calculated with $N = 200$ random sampled topologies are shown in the appendix. We choose “log power” as the extrapolation function family. Fig. 5 shows the leave-one-out ranking correlation comparison of the multi-shot rewards \hat{r} and one-shot rewards. We can see that, compared with one-shot rewards in differently-sized supernet, multi-shot estimated scores are better correlated with the actual scores in each leave-out supernet. This indicates that the correlation gap brought by width difference can be effectively bridged with multi-shot extrapolation.

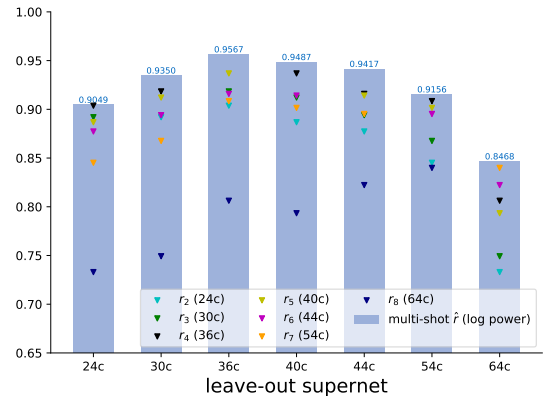


Figure 5. The leave-one-out Spearman ranking correlation. We can see that compared with the one-shot reward in other differently-sized supernet, multi-shot estimated rewards \hat{r} are better correlated with the rewards in the leave-out supernet.

Table 1. Comparison with baseline architectures under various adversarial attacks on CIFAR-10. MSRobNet- C_T indicates the search is targeting at FLOPs C_T . The “-P” suffix indicates stage-wise architectures discovered by predictor-based search (Sec. 6.5).

Architecture	#Param (M)	#FLOPs (M)	Accuracies					Distances (median)	
			Clean	FGSM	PGD ⁷	PGD ²⁰	PGD ¹⁰⁰	DeepFool	BIM
MobileNet-V2	2.30	182	77.0%	53.0%	50.1%	48.0%	47.8%	0.03070	0.03033
ResNet-18	11.17	1110	83.9%	57.9%	54.5%	51.9%	51.5%	0.03976	0.03409
ResNet-50	23.52	2595	85.4%	60.3%	55.9%	52.9%	52.5%	0.04693	0.03533
VGG-16	14.73	626	79.9%	53.7%	50.4%	48.1%	47.9%	0.03254	0.03075
RobNet-free	5.49	1560	82.8%	58.4%	55.1%	52.7%	52.6%	0.03671	0.03466
MSRobNet-1000	3.16	1018	84.9%	59.9%	55.9%	52.8%	52.4%	0.04149	0.03516
MSRobNet-1560	5.30	1588	84.8%	60.0%	56.2%	53.4%	52.9%	0.04323	0.03607
MSRobNet-2000	6.46	2009	85.6%	60.5%	56.5%	53.9%	53.5%	0.04461	0.03600
MSRobNet-1560-P	4.88	1565	85.2%	59.4%	55.2%	51.9%	51.5%	0.04176	0.03493
MSRobNet-2000-P	5.74	2034	86.1%	61.3%	56.9%	53.9%	53.5%	0.04562	0.03635

Table 2. Comparison with architectures discovered by baseline one-shot workflows on CIFAR-10. C_T in “One-shot- \ast - C_T ” indicates that the discovered architecture are augmented to have C_T M FLOPs. All the one-shot search are run in the 44-channel supernet.

Architecture	#Param (M)	#FLOPs (M)	Clean	FGSM	PGD ⁷	PGD ²⁰	PGD ¹⁰⁰
One-shot-rA-1000	3.62	1010	83.9%	58.7%	55.5%	52.9%	52.5%
One-shot-div-1000	3.26	1016	83.6%	58.3%	54.2%	51.4%	51.1%
One-shot-pareto-1000 (1)	3.60	1000	83.8%	59.1%	55.0%	52.2%	51.9%
MSRobNet-1000	3.16	1018	84.9%	59.9%	55.9%	52.8%	52.4%
One-shot-rA-1560	5.65	1571	84.9%	60.0%	56.0%	53.1%	52.6%
One-shot-div-1560	5.00	1552	84.1%	59.1%	55.0%	52.0%	51.6%
One-shot-pareto-1560 (3)	5.18	1562	84.7%	59.4%	55.3%	52.7%	52.5%
MSRobNet-1560	5.30	1588	84.8%	60.0%	56.2%	53.4%	52.9%
One-shot-rA-2000	7.25	2013	85.3%	59.9%	55.9%	53.0%	52.7%
One-shot-div-2000	6.46	2005	85.1%	59.8%	55.9%	52.8%	52.4%
One-shot-pareto-2000 (2)	5.85	1999	85.3%	60.1%	56.1%	53.3%	53.1%
MSRobNet-2000	6.46	2009	85.6%	60.5%	56.5%	53.9%	53.5%

6.3. Results on CIFAR-10

Tab. 1 compares the performances of the architectures under various adversarial attacks. The architectures discovered by our method are referred to as MSRobNet- C_T , in which C_T is the targeted FLOPs in multi-shot search. The table shows that with similar FLOPs, the architectures discovered by multi-shot NAS significantly outperform the manually-designed architectures. For example, at the targeted FLOPs of 2000M, our discovered architectures, MSRobNet-2000 and MSRobNet-2000-P, surpass ResNet-50 consistently by 1% with fewer FLOPs and much fewer parameters. Also, at the targeted FLOPs of 1560M, MSRobNet-1560 (clean 84.8%, PGD¹⁰⁰ 52.9%) outperforms the recent NAS-discovered architecture RobNet-free [9] (clean 82.8%, PGD¹⁰⁰ 52.6%) with similar FLOPs.

We also compare with the architectures discovered by baseline one-shot workflows in Tab. 2. Note that in “One-

shot-pareto” methods, we randomly sample 3 architectures from the pareto front, and only demonstrate the results with the highest natural accuracy for each targeted FLOPs.

Black-box Attacks Tab. 3 shows the results of transfer-based black-box evaluation. Specifically, we train a copy of each of the target models using the same training settings and apply PGD¹⁰⁰ attack on this substitute model to generate adversarial examples. The transferability between different architectures is also studied. We can see that compared to transferring the attacks between the baseline architectures, it is harder to transfer the attacks from baseline architectures to MSRobNets.

6.4. Transfer Results to Other Datasets

We train the discovered architectures on CIFAR-100, SVHN, and Tiny-ImageNet. Tab. 4 and Tiny-ImageNet results in the appendix show that MSRobNets outperform the

Table 3. Black-box PGD¹⁰⁰ attack results on CIFAR-10. Adversarial examples are crafted on an independently trained substitute model, and then used to attack the target model. In this table, “MSRN” is the abbreviation for “MSRobNet”.

Target/Substitute	VGG-16	ResNet-18	MobileNet-V2	MSRN-1560	MSRN-2000	MSRN-1560-P	MSRN-2000-P
VGG-16	56.7%	58.6%	60.0%	59.7%	59.9%	59.8%	60.2%
ResNet-18	62.5%	59.3%	64.7%	61.1%	61.3%	61.3%	61.5%
MobileNet-V2	57.8%	58.0%	54.7%	58.8%	59.0%	58.7%	59.0%
MSRN-1560	66.2%	63.4%	67.3%	61.5%	62.2%	62.4%	61.6%
MSRN-2000	66.6%	64.1%	68.0%	62.8%	61.6%	62.9%	62.7%
MSRN-1560-P	65.6%	62.6%	67.0%	62.2%	61.8%	61.8%	62.0%
MSRN-2000-P	67.3%	64.7%	68.6%	63.1%	63.2%	63.3%	62.0%

Table 4. Comparison with baseline architectures under various adversarial attacks on CIFAR-100 and SVHN.

Architecture	#Param, #FLOPs (M)	CIFAR-100					SVHN				
		Clean	FGSM	PGD ⁷	PGD ²⁰	PGD ¹⁰⁰	Clean	FGSM	PGD ⁷	PGD ²⁰	PGD ¹⁰⁰
VGG-16	14.73, 626	49.2%	23.7%	20.9%	19.0%	18.7%	88.7%	59.2%	53.7%	49.2%	48.2%
ResNet-18	11.17, 1100	54.8%	24.2%	21.2%	19.3%	18.9%	91.0%	63.5%	54.8%	49.0%	47.7%
MobileNet-V2	2.30, 182	53.4%	27.5%	25.7%	24.0%	23.9%	87.9%	59.1%	53.0%	48.4%	47.3%
MSRobNet-1000	3.16, 1019	57.8%	31.5%	29.6%	28.1%	28.0%	90.1%	64.5%	58.5%	54.9%	54.3%
MSRobNet-1560	5.30, 1588	60.3%	32.5%	30.7%	28.9%	28.7%	91.5%	65.5%	57.1%	52.7%	51.0%

Table 5. One-shot rewards & FLOPs and multi-shot rewards of the stage-wise architectures discovered by predictor-based search.

Topology	Search Reward	One-shot Rewards / FLOPs (M)				Multi-shot Rewards	
		r_2 (24c)	r_5 (44c)	r_7 (54c)	r_8 (64c)	\hat{r}_{1560}	\hat{r}_{2000}
one-shot-rA-24c-P	r_2 (24c)	0.594 / 329	0.623 / 1037	0.630 / 1539	0.636 / 2140	0.631	0.634
one-shot-rA-44c-P	r_5 (44c)	0.580 / 340	0.624 / 1072	0.639 / 1592	0.642 / 2213	0.635	0.642
MSRobNet-1560-P	\hat{r}_{1560}	0.569 / 253	0.619 / 805	0.638 / 1196	0.645 / 1666	0.645	0.652
MSRobNet-2000-P	\hat{r}_{2000}	0.572 / 261	0.620 / 826	0.646 / 1228	0.648 / 1708	0.649	0.660

baseline architectures, with comparable FLOPs and fewer parameters.

Another observation is that MSRobNet-1000 outperforms MSRobNet-1560 in adversarial accuracies on SVHN/Tiny-ImageNet, which is different from the results on CIFAR-10/CIFAR-100. This may arise from that larger dataset difference degrades the architecture transferability. Thus, MSRobNet-1560 (discovered on CIFAR-10) is sub-optimal on SVHN/Tiny-ImageNet for the targeted FLOPs.

6.5. Predictor-based Search with Efficient Proxies

In the predictor-based search process, we first randomly sample 200 stage-wise topologies and train the initial predictor. Then, we run the predictor-based search for eight steps, and in each step, 50 topologies are sampled by the predictor-based controller and evaluated using the multi-shot strategy. Then the evaluation results are used to tune the predictor. The search process can be finished in 1.3 GPU days on a 2080Ti GPU.

We conduct the predictor-based search process using our multi-shot rewards targeting two FLOPs (1560M, 2000M), and the discovered topologies are named MSRobNet-1560-

P and MSRobNet-2000-P, respectively. We augment these two topologies to 1560M and 2000M, respectively, and their final performances on CIFAR-10 are shown in Tab. 1.

For comparison, we conduct predictor-based search using two baseline one-shot-rA rewards r_2 (supernet with 24 init channel) and r_5 (supernet with 44 init channel). Tab. 5 illustrates the one-shot rewards/FLOPs and multi-shot rewards of topologies discovered with different search rewards. We can see that one-shot methods prefer topologies with larger one-shot capacity, and these topologies can no longer be superior when augmented to a different targeted capacity C_T . For example, the topology *one-shot-rA-24c-P* discovered using reward r_2 has the highest $r_2 = 0.594$. However, in the 64-init-channel supernet, it only achieves $r_8 = 0.636$ with 2140M FLOPs, while MSRobNet-2000-P achieves $r_8 = 0.648$ with a smaller FLOPs of 1708M. That is to say, when the targeted capacity is 2000M, MSRobNet-2000-P is superior to *one-shot-rA-24c-p*.

7. Conclusion

This paper proposes a multi-shot neural architecture search (multi-shot NAS) framework to discover adversar-

ially robust architectures at targeted capacities. Instead of using one supernet in one-shot NAS, multiple supernets with different capacities are constructed and trained. By evaluating each topology with the inter- or extra-polation of multiple rewards, we can explicitly search for superior architectures for a targeted capacity. Experimental results demonstrate the effectiveness of the proposed method.

Furthermore, the multi-shot evaluation methodology can be extended beyond the search for adversarial robustness. In other scenarios with a targeted capacity, or for other objectives that are sensitive to the capacity misalignment issue, the multi-shot methodology can be applied to achieve a balance between the impreciseness of one-shot methods and the inefficiency of methods with separate training phases.

References

- [1] Anish Athalye, Nicholas Carlini, and David Wagner. Obfuscated gradients give a false sense of security: Circumventing defenses to adversarial examples. *arXiv preprint arXiv:1802.00420*, 2018. [2](#)
- [2] Gabriel Bender, P. Kindermans, Barret Zoph, V. Vasudevan, and Quoc V. Le. Understanding and simplifying one-shot architecture search. In *ICML*, 2018. [3](#)
- [3] Nicholas Carlini and David Wagner. Adversarial examples are not easily detected: Bypassing ten detection methods. In *Proceedings of the 10th ACM Workshop on Artificial Intelligence and Security*, pages 3–14, 2017. [2](#)
- [4] Nicholas Carlini and David Wagner. Towards evaluating the robustness of neural networks. In *2017 IEEE Symposium on Security and Privacy (SP)*, pages 39–57. IEEE, 2017. [2](#), [16](#)
- [5] Hanlin Chen, B. Zhang, Song Xue, Xuan Gong, Hong-Chen Liu, Rongrong Ji, and D. Doermann. Anti-bandit neural architecture search for model defense. *ArXiv*, abs/2008.00698, 2020. [2](#), [15](#)
- [6] Moustapha Cisse, Piotr Bojanowski, Edouard Grave, Yann Dauphin, and Nicolas Usunier. Parseval networks: Improving robustness to adversarial examples. In *Proceedings of the 34th International Conference on Machine Learning-Volume 70*, pages 854–863. JMLR. org, 2017. [1](#), [2](#)
- [7] Ian J. Goodfellow, Jonathon Shlens, and Christian Szegedy. Explaining and harnessing adversarial examples. *CoRR*, abs/1412.6572, 2015. [2](#), [6](#)
- [8] Chuan Guo, Mayank Rana, Moustapha Cisse, and Laurens van der Maaten. Countering adversarial images using input transformations. In *International Conference on Learning Representations*, 2018. [1](#), [2](#)
- [9] Minghao Guo, Yuzhe Yang, Rui Xu, and Ziwei Liu. When nas meets robustness: In search of robust architectures against adversarial attacks. *arXiv preprint arXiv:1911.10695*, 2019. [2](#), [3](#), [4](#), [5](#), [7](#), [15](#), [17](#)
- [10] Kirthevasan Kandasamy, Willie Neiswanger, Jeff Schneider, Barnabas Poczos, and Eric P Xing. Neural architecture search with bayesian optimisation and optimal transport. In *Advances in Neural Information Processing Systems*, pages 2016–2025, 2018. [3](#)
- [11] A. Krizhevsky. Learning multiple layers of features from tiny images. 2009. [6](#)
- [12] Alexey Kurakin, Ian Goodfellow, and Samy Bengio. Adversarial machine learning at scale. *arXiv preprint arXiv:1611.01236*, 2016. [2](#)
- [13] A. Kurakin, Ian J. Goodfellow, and S. Bengio. Adversarial examples in the physical world. *ArXiv*, abs/1607.02533, 2017. [6](#), [16](#)
- [14] Hanxiao Liu, Karen Simonyan, and Yiming Yang. Darts: Differentiable architecture search. *arXiv preprint arXiv:1806.09055*, 2018. [1](#), [2](#), [3](#)
- [15] Renqian Luo, Fei Tian, Tao Qin, Enhong Chen, and Tie-Yan Liu. Neural architecture optimization. In *Advances in Neural Information Processing Systems 31*, pages 7816–7827. 2018. [3](#)
- [16] Aleksander Madry, Aleksandar Makelov, Ludwig Schmidt, Dimitris Tsipras, and Adrian Vladu. Towards deep learning models resistant to adversarial attacks. In *International Conference on Learning Representations*, 2018. [1](#), [2](#), [3](#), [4](#), [6](#)
- [17] Jan Hendrik Metzen, Tim Genewein, Volker Fischer, and Bastian Bischoff. On detecting adversarial perturbations. *arXiv preprint arXiv:1702.04267*, 2017. [2](#)
- [18] Seyed-Mohsen Moosavi-Dezfooli, Alhussein Fawzi, and Pascal Frossard. Deepfool: a simple and accurate method to fool deep neural networks. In *Proceedings of the IEEE conference on computer vision and pattern recognition*, pages 2574–2582, 2016. [2](#), [6](#), [16](#)
- [19] Yuval Netzer, T. Wang, A. Coates, Alessandro Bissacco, B. Wu, and A. Ng. Reading digits in natural images with unsupervised feature learning. 2011. [6](#)
- [20] Xuefei Ning, Yin Zheng, Tianchen Zhao, Yu Wang, and Huazhong Yang. A generic graph-based neural architecture encoding scheme for predictor-based nas. In *The European Conference on Computer Vision (ECCV)*, 2020. [3](#), [5](#), [14](#), [15](#)
- [21] Tianyu Pang, Xiao Yang, Yinpeng Dong, Hang Su, and Jun Zhu. Bag of tricks for adversarial training. *arXiv preprint arXiv:2010.00467*, 2020. [14](#)
- [22] Nicolas Papernot, Patrick McDaniel, Somesh Jha, Matt Fredrikson, Z Berkay Celik, and Ananthram Swami. The limitations of deep learning in adversarial settings. In *2016 IEEE European symposium on security and privacy (EuroS&P)*, pages 372–387. IEEE, 2016. [2](#)
- [23] Nicolas Papernot, Patrick McDaniel, Xi Wu, Somesh Jha, and Ananthram Swami. Distillation as a defense to adversarial perturbations against deep neural networks. In *2016 IEEE Symposium on Security and Privacy (SP)*, pages 582–597. IEEE, 2016. [2](#)
- [24] Hieu Pham, Melody Y Guan, Barret Zoph, Quoc V Le, and Jeff Dean. Efficient neural architecture search via parameter sharing. *arXiv preprint arXiv:1802.03268*, 2018. [1](#), [2](#), [3](#)
- [25] Jonas Rauber, Wieland Brendel, and Matthias Bethge. Foolbox: A python toolbox to benchmark the robustness of machine learning models. In *Reliable Machine Learning in the Wild Workshop, 34th International Conference on Machine Learning*, 2017. [6](#), [16](#)
- [26] Esteban Real, Alok Aggarwal, Yanping Huang, and Quoc V Le. Regularized evolution for image classifier architecture search. In *Proceedings of the aaai conference on artificial intelligence*, volume 33, pages 4780–4789, 2019. [2](#), [5](#), [12](#)
- [27] L Schott, J Rauber, M Bethge, and W Brendel. Towards the first adversarially robust neural network model on mnist. In *Seventh International Conference on Learning Representations (ICLR 2019)*, pages 1–16, 2019. [1](#)
- [28] Yang Song, Taesup Kim, Sebastian Nowozin, Stefano Ermon, and Nate Kushman. Pixeldefend: Leveraging generative models to understand and defend against adversarial examples. In *International Conference on Learning Representations*, 2018. [1](#), [2](#)
- [29] Christian Szegedy, V. Vanhoucke, S. Ioffe, Jon Shlens, and Z. Wojna. Rethinking the inception architecture for computer vision. *2016 IEEE Conference on Computer Vision and Pattern Recognition (CVPR)*, pages 2818–2826, 2016. [14](#)

- [30] Christian Szegedy, Wojciech Zaremba, Ilya Sutskever, Joan Bruna, Dumitru Erhan, Ian Goodfellow, and Rob Fergus. Intriguing properties of neural networks. *arXiv preprint arXiv:1312.6199*, 2013. [1](#)
- [31] Hongyang Zhang, Yaodong Yu, Jiantao Jiao, Eric Xing, Laurent El Ghaoui, and Michael Jordan. Theoretically principled trade-off between robustness and accuracy. In *International Conference on Machine Learning*, pages 7472–7482, 2019. [1](#), [2](#)
- [32] Barret Zoph and Quoc V. Le. Neural architecture search with reinforcement learning. In *ICLR*, 2017. [2](#)

Appendix A. Extrapolation Function Family Selection

The 7 parametric saturating function families are

1. Janoschek: $f(x; a, b, c, d) = a - (a - b)e^{-cx^d}$
2. vapor pressure: $f(x; a, b, c) = e^{a + \frac{b}{x} + c \log(x)}$
3. log log linear: $f(x; a, b) = \log(a \log(x) + b)$
4. ilog2: $f(x; a, c) = c - \frac{a}{\log(x)}$
5. log power: $f(x; a, b, c) = \frac{a}{1 + (x/e^b)^c}$
6. MMF: $f(x; a, b, c, d) = a - \frac{a-b}{1 + (dx)^c}$
7. log power rep: $f(x; a, b, c) = \frac{1}{(1 + e^{-a})(1 + e^{cx}e^{-b})}$

The leave-one-out function selection scheme is summarized in Alg. 2. In practice, we find that all the candidate function families have a weak correlation between estimated and actual one-shot rewards in χ_1 (supernet with init channel number 12). In addition, the capacity of χ_1 is so small that FLOPs of almost all the topologies in it are far from the targeted capacity. Thus, we regard the estimation results in χ_1 as outliers, and do not include $\tau_1^{(i)}$ when calculating $\bar{\tau}^{(i)} = \frac{1}{K-1} \sum_{j=2}^K \tau_j^{(i)}$.

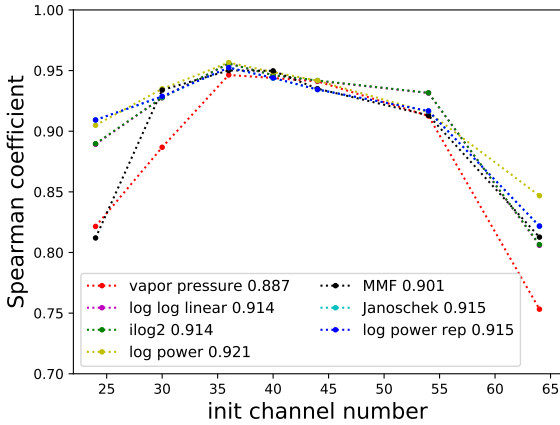


Figure A1. The leave-one-out Spearman ranking correlation curves of 7 function families (200 random sampled topologies are used). Their average leave-one-out correlation coefficients $\bar{\tau}^{(i)}$ s are shown in the legend.

The leave-one-out correlations are shown in Fig. A1. We choose “log power” as the extrapolation function family, since it has the highest average leave-one-out correlation (0.921).

Tab. 5 in the main text gives some evidence on our motivation. To give a more intuitive evidence on the motivation example in the main text, we show the extrapolation

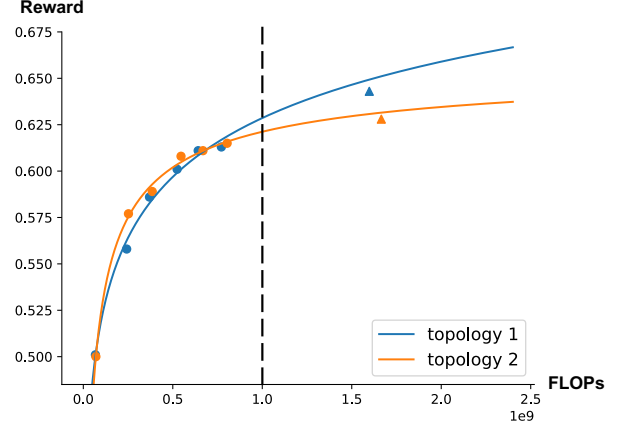


Figure A2. Reward extrapolation example. The markers on one curve denote the topology’s rewards evaluated in differently-sized supernets.

curves of two topologies (among the 200 randomly sampled topologies in our experiment) in Fig. A2. We can see that when aligned to the same capacity (FLOPs), topology 2 is more robust in the low-capacity region, while topology 1 is more robust in the high-capacity region. The two curves are fitted using the data points at the left of the dashed line. And we can see that the fitted curve can capture the tendency, thus manage to predict the relative ranking correctly at a larger capacity without actual training a large supernet (the leftmost triangular markers).

Appendix B. Experimental Setup

B.1. Search Strategy Settings

Evolutionary Search The search strategy is a tournament-based evolutionary method [26], with population size 100 and tournament size 10. A difference is that the elimination strategy is to remove the worst topology in the population, instead of removing the oldest one.

Predictor-based Search with Efficient Proxies The predictor-based search process is summarized in Alg. 1. We first randomly sample 200 stage-wise architectures, evaluate them, and train the initial predictor (Line 21). Then, the predictor-based search is run for $T^p = 8$ stages. In each stage, $N^p = 50$ architectures are sampled by the predictor-based controller (Line 23) and evaluated using the multi-shot strategy (Line 24). And then, the multi-shot evaluation results are used to tune the predictor (Line 25).

In the inner search process (Line 23), we run a tournament-based evolutionary search with population size 20 and tournament size 5. We conduct $N^p \times 50$ evolutionary search steps, and in each step, a mutated topology is assessed by the predictor, which is very efficient. And in every 50 steps, a topology with the highest predicted score

Algorithm 1: Multi-shot Architecture Search for Adversarial Robustness

Input:

- *Data & Attack*: train-valid split ratio $s = 0.8$, PGD attack steps $T^a = 7$, perturbation budget $\epsilon = 0.031$, attack step size $\eta = 0.0078$
- *Supernet training*: number of supernet $K = 8$, supernet init channel numbers $\{c_1^s, \dots, c_K^s\}$, training epochs $T^s = 400$
- *Function Family Selection*: number of randomly sampled topologies $N = 200$, candidate function families $F = \{f^1, \dots, f^7\}$
- *Search*: targeted capacity C_T
 - Evolutionary: search steps $T^e = 200$, population size $\pi = 100$, tournament size $\mu = 10$, PGD attack steps $T^{sa} = 7$
 - Predictor-based: search stages $T^p = 8$, topologies sampled per stage $N^p = 50$, inner evolutionary search steps $T^{pe} = N^p \times 50 = 2500$, PGD attack steps $T^{sa} = 1$ (FGSM, no random init)

Output: A discovered topology.

```
1  $s$  of the training dataset as the training split  $D_t$ , reset as the validation split  $D_v$ 
   /* Adversarially train the supernet */
2 for  $i = 1 \dots K$  do
3    $\chi_i, w_i \leftarrow \text{INIT-SUPERNET}(c_i^s)$ 
4   for  $j = 1 \dots T^s$  do
5     for  $x_t, y_t$  in  $D_t$  do
6        $\alpha \sim \mathcal{A}$  /* random arch. sample */
7        $x' \leftarrow \text{PGD}(x_t, y_t, \chi_i(\alpha, w_i); T^a, \epsilon, \eta)$ 
8        $L = \text{CE}(\chi_i(\alpha, w_i)(x'), y_t)$ 
9        $w_i \leftarrow \text{SGD-UPDATE}(w_i, \nabla_{w_i} L)$ 
10 Select the extrapolation function family  $f \in F$  based on the leave-one-out ranking correlations, using  $N$  randomly sampled topologies
11 if EVO Search then
12   /* Evolutionary Search with multi-shot evaluation */
13   pop  $\leftarrow \{\pi \text{ topologies with the highest rewards in the } N \text{ random sampled topologies, together with their multi-shot estimated rewards at } C_T\}$ 
14   for  $t = 1 \dots T^e$  do
15     pool  $\leftarrow$  set of  $\mu$  randomly choosed topologies from the pop
16     parent  $\leftarrow$  topologies with the best reward in pool
17      $\alpha_t \leftarrow \text{MUTATION}(\text{parent})$ 
18     Add  $(\alpha_t, \text{MultiShotEval}(\alpha_t, C_T, f, T^{sa}))$  to pop
19     Remove the worst topology in pop
19 else if Predictor-based search then
20   /* Predictor-based Search with multi-shot evaluation */
21   pop  $\leftarrow \{\text{the } N \text{ random sampled topologies, together with their multi-shot estimated rewards at } C_T\}$ 
22   Train  $P$  using pop
23   for  $t = 1 \dots T^p$  do
24      $\{\alpha_i^{(t)}\}_{i=1, \dots, N^p} \sim$  evolutionary inner search for  $T^{pe}$  steps using the predictor  $P$ 
25     Get their multi-shot estimated rewards  $\{(\alpha_i^{(t)}, \text{MultiShotEval}(\alpha_i^{(t)}, C_T, f, T^{sa}))\}_{i=1, \dots, N^p}$ , and add to pop
26     Tune  $P$  with the newly evaluated topologies
26 Return topology with highest multi-shot estimated reward in the population pop
```

Algorithm 2: Leave-One-Out Function Selection

Input: Candidate Function Families $F = \{f^{(i)}\}_{i=1, \dots, 7}$

Output: A function family f^*

Parameter: Number of supernet $K = 8$, number of topologies $N = 200$

```
1 Random sample  $N$  architectures  $\{\alpha_n\}_{n=1, \dots, N}$  from the search space
2 for  $j = 1 \dots K$  do
3   | Get the one-shot capacities and rewards  $\{(C_j(\alpha_n), r_j(\alpha_n))\}_{n=1, \dots, N}$ 
4 for  $j = 1 \dots K$  do
5   | /* Get leave- $j$  out correlation */
6   | for  $i = 1 \dots 7$  do
7   |   | for  $n = 1 \dots N$  do
8   |     |  $\beta_j^{(i)}(\alpha) = \text{Fit}(f^{(i)}, \{r_m(\alpha)\}_{m=1, \dots, K, m \neq j}, \{C_m(\alpha)\}_{m=1, \dots, K, m \neq j})$ 
9   |     |  $\hat{r}_j^{(i)}(\alpha_n) = f_i(\alpha_n; \beta_j^{(i)}(\alpha_n))$ 
10  |     |  $\tau_j^{(i)} = \text{SpearmanR}(\{\hat{r}_j^{(i)}(\alpha_n)\}_{n=1, \dots, N}, \{r_j(\alpha_n)\}_{n=1, \dots, N})$ 
11  $f^* = \arg \max_{f^{(i)} \in F} \bar{\tau}^{(i)} = \arg \max_{f^{(i)} \in F} \sum_{j=2}^K \tau_j^{(i)}$ 
12 Return function family  $f^*$ .
```

Algorithm 3: MultiShotEval: Multi-shot Architecture Evaluation

Input: A candidate topology α_t , targeted capacity C_T , extrapolation function family f , PGD attack steps in adversarial accuracy evaluation T^{sa}

Output: The multi-shot estimated reward $\hat{r}(\alpha_t)$ at capacity C_T

Parameter: Accuracy coefficient $\lambda = 0.5$

```
1 for  $i = 1 \dots K$  do
2   |  $w_i \leftarrow \text{CALIB-BN}(\alpha_t, w_i, D_v)$ 
3   |  $r_i(\alpha_t) = (1 - \lambda)\text{Acc}_{\text{clean}}(\chi_i(\alpha_t, w_i), D_v, y_v) + \lambda\text{Acc}_{\text{pgd}}(\chi_i(\alpha_t, w_i), D_v, y_v; T^{sa}, \epsilon, \eta)$ 
4  $\hat{\beta}(\alpha_t) = \text{Fit}(f, \{r_i(\alpha_t)\}_{i=1 \dots K}, \{C_i(\alpha_t)\}_{i=1 \dots K})$ 
5  $\hat{r}(\alpha_t) = f(C_T; \hat{\beta}(\alpha_t))$ 
6 Return  $\hat{r}(\alpha_t)$ 
```

in the current population is decided for the actual multi-shot evaluation. In each step, the topology with the lowest predicted score is removed from the population.

As for the predictor construction, we use a graph-based encoder [20] to encode the topology of each cell into a continuous vector, and then concatenate the embeddings of four cell topologies (S0, S1, S2, R) as the architecture embedding. Then the architecture embedding is fed into an MLP to get a predicted score. The operation embedding dimension, node embedding dimension, and hidden dimension are all 48. And the output dimension of each cell topology is set to 32. Thus, the dimension of one full topology is 128. Then this 128-dim vector is fed into a 3-layer MLP with 256 hidden units and output a final score. In each predictor training process, the predictor is trained for 100 epochs with batch size 50 and an Adam optimizer (1e-3 learning rate). We use

hinge pair-wise ranking loss with margin $m = 0.1$ to train the predictor following [20]. A dropout of 0.1 before the MLP is used.

B.2. Adversarial Training of Architectures

For the final comparison of all the architectures, we adversarially train them for 110 epochs using PGD⁷ attacks with $\epsilon = 0.031(8/255)$ and step size $\eta = 0.0078(2/255)$. The batch size is set to 48, and we use an SGD optimizer with momentum 0.9, gradient clipping 5.0, and weight decay 5e-4. The learning rate is set to 0.05 initially and decayed by 10 at epoch 100 and epoch 105. In addition, following a recent study [21], we employ the label smoothing regularization [29] with weight 0.2. No cutout and dropout is applied. All models are trained with the same settings on a single 2080Ti GPU.

On Tiny-ImageNet, the image size is 64×64 instead of 32×32 , and we change the stem from a 3×3 convolution to a 7×7 convolution with stride 2. Due to this modification, the overall FLOPs is still close to C_T . For all the architectures, we first conduct a normal training process for 110 epochs with batch size 256. The learning rate is set to 0.1 initially and decayed by 10 at epoch 30, 60 and 100. Using the normally-trained model as the pre-trained model, we adversarially train the model for 70 epochs with PGD⁵ attack ($\epsilon = 0.0157(4/255)$, step size $\eta = 0.0039(1/255)$). The learning rate is linearly warmed up from 0 to 0.05 in 10 epochs, and decayed by 10 at epoch 45 and 60. In both the normal and adversarial training processes, an SGD optimizer with momentum 0.9, gradient clipping 5.0, and weight decay $3e-4$ is used.

Appendix C. Additional Experimental Results

C.1. Transfer Results to Tiny-ImageNet

We compare two baseline architectures (ResNet-18, ResNet-50), and the MSRobNet-1000 and MSRobNet-1560 architectures on Tiny-ImageNet. Tab. A1 shows that MSRobNets outperform the baseline architectures, with comparable FLOPs and fewer parameters.

As also been discussed in the main text, MSRobNet-1000 outperforms MSRobNet-1560 in adversarial accuracies on Tiny-ImageNet, which is different from the results on CIFAR-10/CIFAR-100. We attribute this observation to that the larger dataset difference between CIFAR-10 and Tiny-ImageNet degrades the architecture transferability. Thus, MSRobNet-1560 discovered on CIFAR-10 is suboptimal on Tiny-ImageNet for the targeted FLOPs of 1560M.

C.2. BatchNorm Calibration

Fig. A3 shows that without BatchNorm calibration (No CalibBN, green points), the evaluation results are unmeaningful. And after BN calibration with several batches, the accuracies and rankings of 200 randomly sampled sub-architectures become meaningful. Note that we calculate the ranking correlation with the CalibBN-15 results (calibration using 15 batches), since we fail to tune the architectures to the same level of accuracies with only 3 epochs of training as in [9].

Appendix D. Discussion

D.1. Adversarial Robustness Evaluation in the Search Phase: PGD V.S. FGSM

Compared with normal training and evaluation, adversarial training and adversarial robustness evaluation are much more time-consuming. Since NAS itself faces the computational challenge, how to evaluate the adversarial ro-

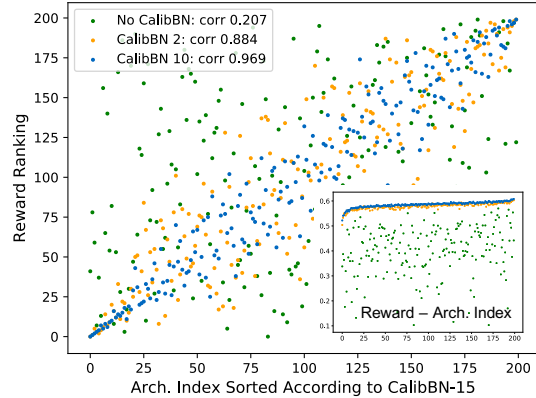


Figure A3. The effect of BatchNorm calibration.

business efficiently in the search phase is an important problem. We wonder whether we can use a weaker and faster attack in the search phase while still managing to discover a robust architecture under the stronger attack. For example, while the final comparison is conducted using PGD⁷ (PGD attack with 7 steps), a recent study [5] tried to use the weaker FGSM attack during the whole search phase for efficiency.

As described in the main text, the search phase includes the supernet training phase and the parameter-sharing search phase. We conduct the following experiments to verify whether it is suitable to use FGSM as a substitute in the search phase: 1) FGSM-FGSM: Train another supernet with FGSM adversarial training, and use FGSM to evaluate the 200 randomly sampled topologies. 2) PGD⁷-FGSM: Reuse the supernet trained with PGD⁷ adversarial training, but use FGSM to evaluate the 200 randomly sampled topologies. The notation “ATTACK1-ATTACK2” means that “ATTACK1” is used in supernet adversarial training and “ATTACK2” is used in the parameter-sharing evaluation, and the step size of the FGSM attack is set to $8/255$. Fig. A4 shows the rankings of these evaluations and the Spearman coefficient with the PGD⁷-PGD⁷ evaluations. The results show that using a much weaker attack FGSM for adversarial training causes the supernet evaluation to be uncorrelated. Thus, one can use FGSM for acceleration during the parameter-sharing search phase, while should keep using a stronger attack during the supernet training phase.

In the stage-wise search space, we also calculate the Kendall Tau, Spearman correlation, and P@K [20] of using PGD⁷-FGSM as a proxy reward for PGD⁷-PGD⁷. The P@K criterion reports the proportion of topologies with top-K rewards evaluated by PGD⁷-FGSM in the top-K topologies evaluated by PGD⁷-PGD⁷, and is a criterion that focus more on well-performing topologies. Results in Tab. A2 show that most of the high-score topologies evalu-

Table A1. Comparison with baseline architectures under various adversarial attacks on Tiny-ImageNet.

Architecture	#Param, #FLOPs (M)	Clean	FGSM	PGD ⁵	PGD ²⁰	PGD ¹⁰⁰
ResNet-18	11.28, 1126	50.3%	27.1%	28.8%	24.4%	24.3%
ResNet-50	23.92, 2612	52.2%	27.8%	29.4%	25.2%	25.0%
MSRobNet-1000	3.33, 1056	52.3%	28.7%	30.6%	26.5%	26.4%
MSRobNet-1560	5.51, 1633	52.9%	28.1%	29.7%	25.9%	25.6%

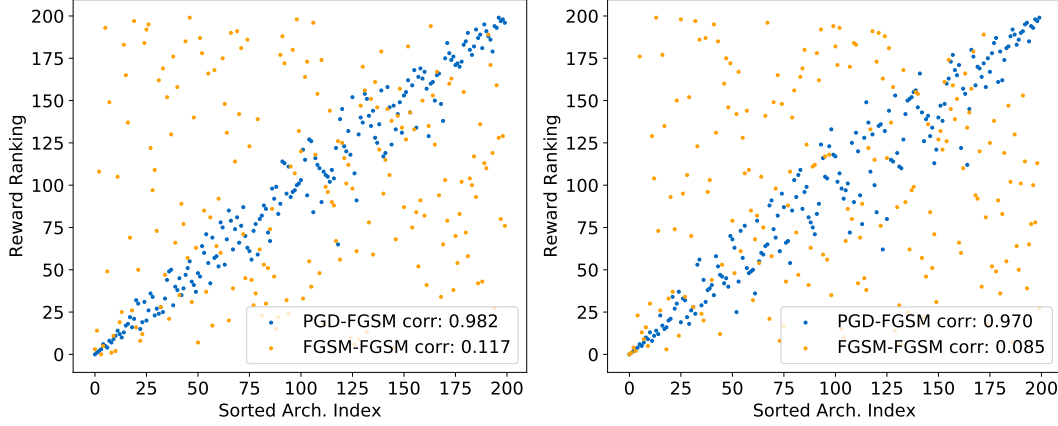


Figure A4. X axis: Indices of architectures sorted according to reward ranking evaluated by PGD⁷-PGD⁷. Y axis: The reward rankings evaluated by PGD⁷-FGSM and FGSM-FGSM. The legends show the Spearman correlation of the rewards and the PGD⁷-PGD⁷ rewards. Left: 24 init channel; Right: 36 init channel.

ated by PGD⁷-FGSM also perform well under PGD⁷-PGD⁷ evaluation, which demonstrates that FGSM is indeed a suitable proxy attack for PGD during the search phase.

D.2. Adversarial Robustness Evaluation in the Search Phase: Distance-based Criterion

In our paper, we use a reward formulation that is a weighted sum of clean and adversarial accuracies.

$$r = \lambda acc_{adv} + (1 - \lambda) acc_{clean}, \quad (6)$$

where λ is a hyperparameter making a trade-off between the clean and adversarial accuracies. During our search, λ is set to 0.5. In other words, we use the average of clean and adversarial accuracies as the reward to guide the search.

Another type of robustness criterion is the distance-based criteria. The Foolbox toolbox [25] implements various kinds of distance attacks that attempt to find a minimum successful perturbation. Examples that have been misclassified without any adversarial perturbation are assigned zero attack distance. In this way, no averaging coefficient is needed to trade off the clean and adversarial accuracies, since the clean accuracy is handled implicitly.

We try to explore how these different robustness criteria correlate with each other. We evaluate the 200 randomly sampled architectures on the validation dataset in χ_2

(init channel number 24) under five kinds of distance attacks. The five attacks are Basic Iterative Method (BIM) L_2 / L_∞ [13], DeepFool L_2 / L_∞ [18] and C&W L_2 [4], where L_2 or L_∞ denotes the type of the L_p distance measure in the input space. Due to the low efficiency of C&W attack, we only run it on 500 images (1/20) in the validation set. We use the median distance as one architecture’s performance criterion under the preformed attack, since it is insensitive to outliers (e.g., when the attack fails to find a proper adversarial perturbation within limited attack steps). For comparison, we also run PGD⁷ and FGSM attacks and calculate their rewards as in Eq. 6 with $\lambda = 0.5$.

The Kendall Tau correlation coefficients between different criteria are shown in Fig. A5. We can see that

1. Different robustness criteria are indeed correlated.
2. Compared with the relatively high correlation between FGSM and PGD adversarial accuracies and rewards (> 0.8), their correlations with distance criteria are relatively weaker. The clean accuracy is better correlated with FGSM/PGD rewards (0.718, 0.669) than the distance-based criteria (0.366-0.465). This is intuitive since the clean accuracy is added into FGSM/PGD rewards explicitly, while only handled implicitly (attack distance = 0 or > 0) in distance-based attacks. On the other hand, they are all higher than the correlations

Table A2. Kendall Tau, Spearman correlation, and P@K of using PGD⁷-FGSM as a proxy reward for PGD⁷-PGD⁷ in different supernets. 200 randomly sampled stage-wise topologies are used.

Supernet	Kendall Tau	Spearman	P@5	P@10	P@20	P@50	P@100
χ_1	0.904	0.987	0.60	0.80	0.90	0.88	0.94
χ_2	0.862	0.972	0.80	0.90	0.75	0.90	0.92
χ_3	0.859	0.973	0.60	0.60	0.80	0.90	0.94
χ_4	0.832	0.960	0.80	0.70	0.90	0.82	0.94
χ_5	0.867	0.973	0.60	0.90	0.85	0.90	0.93
χ_6	0.858	0.969	0.60	0.90	0.75	0.88	0.91
χ_7	0.835	0.959	0.80	0.90	0.70	0.82	0.93
χ_8	0.830	0.958	0.80	0.80	0.75	0.84	0.90



Figure A5. The correlation of various robustness criteria during the search phase (200 cell-wise topologies are used).

of clean accuracy and FGSM/PGD adversarial accuracies (0.324, 0.282), which verifies that an implicit or explicit trade-off between clean and adversarial accuracies must be considered in the robustness criterion.

- Intuitively, compared with L_∞ attack distances, L_2 attack distances are better correlated with other L_2 attack distances, and vice versa. For example, $\text{Corr}(\text{DeepFool } L_\infty, \text{BIM } L_\infty) = 0.724 > \text{Corr}(\text{DeepFool } L_\infty, \text{BIM } L_2) = 0.644$. There are indeed differences brought by input space measure, and this motivates us to use criteria with different input space measure to assess model robustness.

- FGSM/PGD attacks are conducted with L_∞ input space measure, thus the correlation of their rewards with L_∞ attack distances is higher than L_2 attack dis-

tances.

D.3. Efficiency

After been trained only once, the supernets can be reused to discover architectures targeting different capacities (e.g., 1000M, 1560M, 2000M), or in search space with different macro layouts (e.g., cell-wise, stage-wise). Thus, for each targeted capacity, denoting the epoch-wise training and evaluation time of one architecture as t^s and t^e , the search time can be estimated as $(N + T^e)Kt^e$. By using the BatchNorm calibration technique, we obviate the need of separate architecture training phases during the search. If each architecture needs to be finetuned for n epochs (e.g., $n = 3$ in [9]), the search time becomes $(\pi + T^e)(t^e + nt^s)$. We can estimate the coefficients of T^e in the multi-shot method and a NAS method with separate training phases as $Kt^e \approx 8t^e$ and $t^e + nt^s \approx 25t^e$, respectively.¹ This means that, compared with the NAS methods that have separate training phases, the relative efficiency of multi-shot NAS emerges as the number of explored architectures increases.

In the more efficient predictor-based search flow, the FGSM proxy reward and fewer validation images accelerate the evaluation process by roughly $8\times$ (from 25 min to 3 min for evaluating each topology on a single 2080Ti GPU). In total, $N + T^p \times N^p = 200 + 400 = 600$ topologies are assessed using the multi-shot evaluation strategy, and the whole search process can be finished in 1.3 GPU days.

Appendix E. Discovered Architectures

The discovered cell-wise architectures, MSRobNet-1000, MSRobNet-1560 and MSRobNet-2000, are shown in Fig. A6, Fig. A7, and Fig. A8, respectively. The discovered stage-wise architectures, MSRobNet-1560-P and MSRobNet-2000-P, are shown in Fig. A9 and Fig. A10, respectively.

¹In our experiments, we find that t^s/t^e is approximately 2 times of the train-valid data portion ratio $t^s/t^e \approx 2s/(1-s) = 8$.

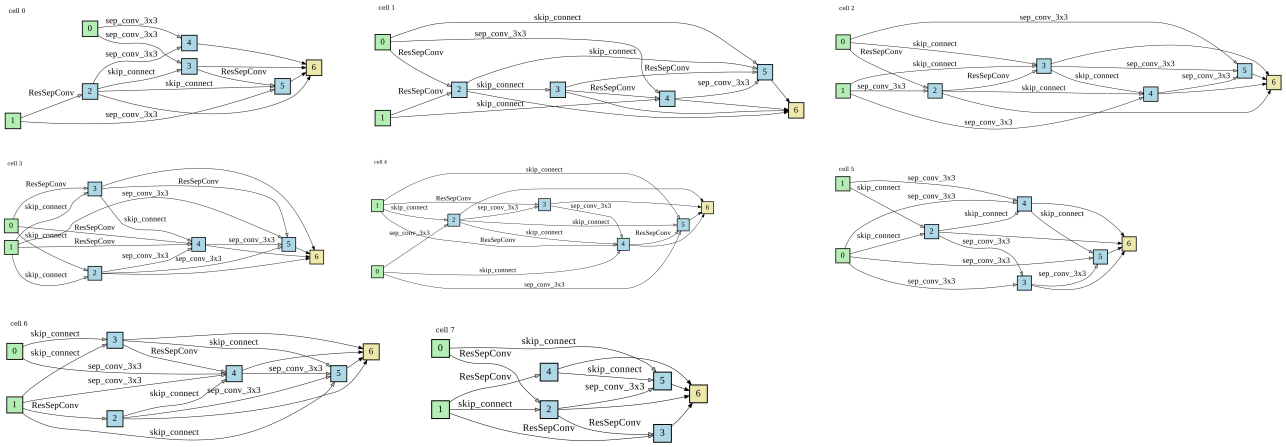


Figure A6. Architecture of MSRobNet-1000.

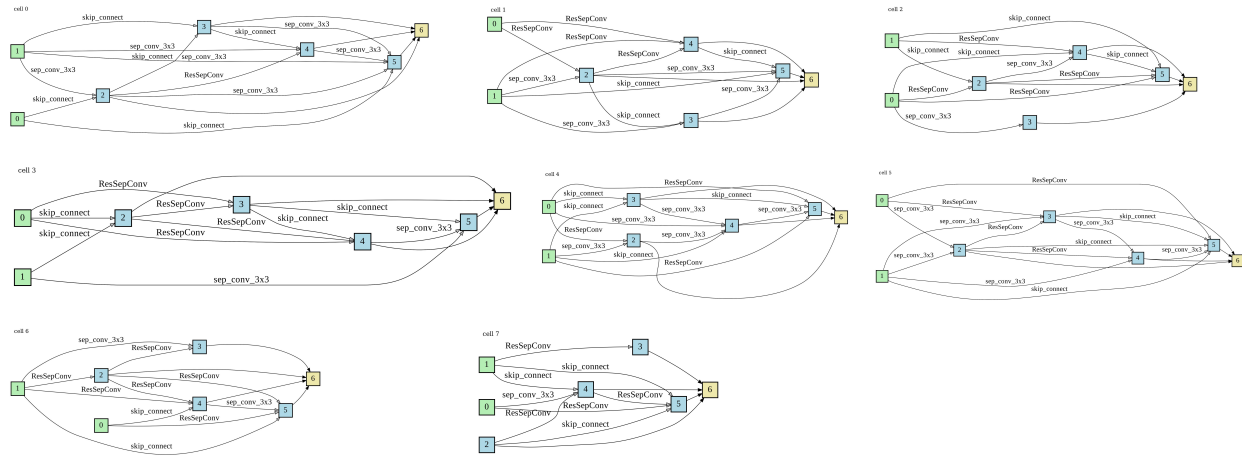


Figure A7. Architecture of MSRobNet-1560.

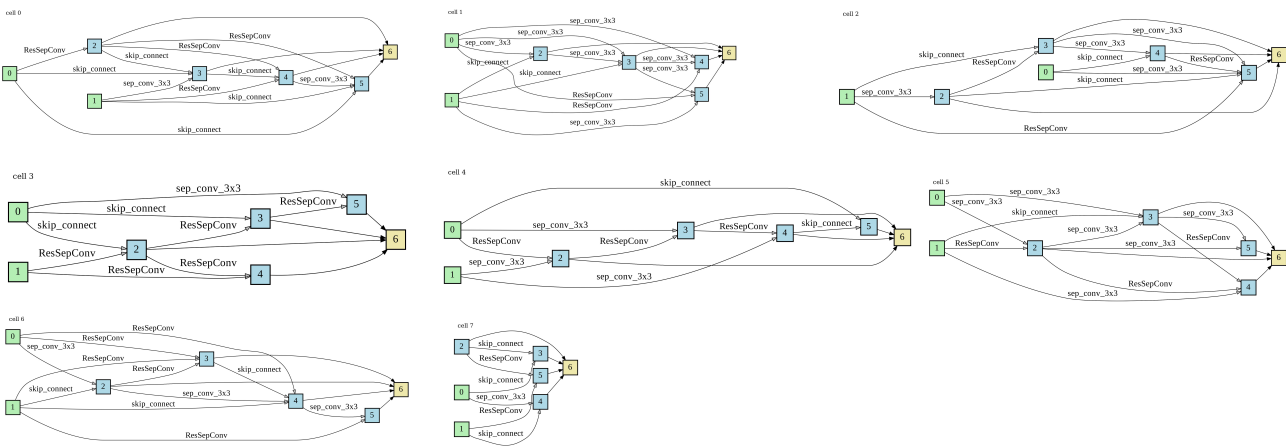
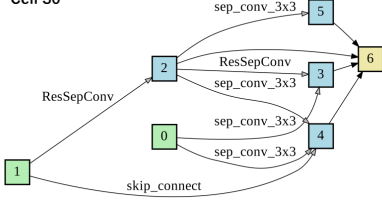
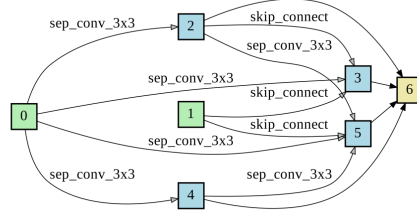


Figure A8. Architecture of MSRobNet-2000.

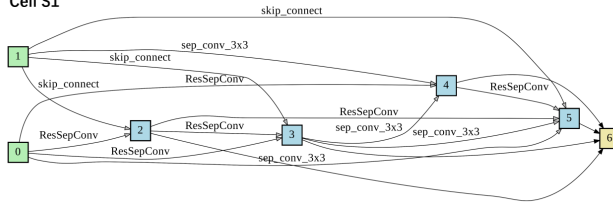
Cell S0



Cell R



Cell S1



Cell S2

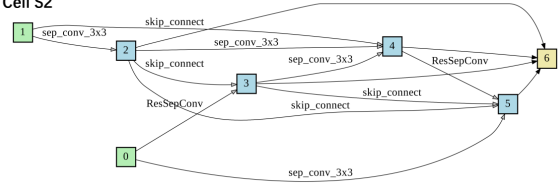
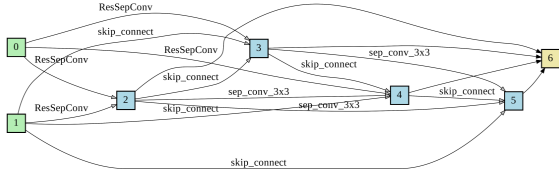
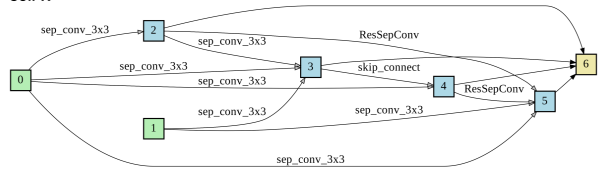


Figure A9. Architecture of MSRobNet-1560-P.

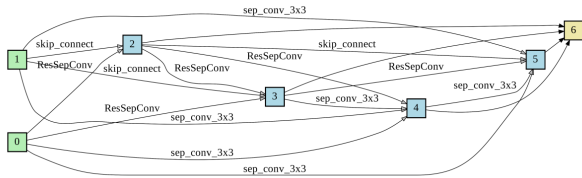
Cell S0



Cell R



Cell S1



Cell S2

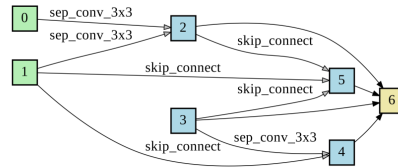


Figure A10. Architecture of MSRobNet-2000-P.